

1 Generation of autogenic knickpoints in laboratory landscape  
2 experiments evolving under constant forcing.

3

4 **Léopold de Lavaissière<sup>1</sup>, Stéphane Bonnet<sup>1</sup>, Anne Guyez<sup>1</sup>, and Philippe Davy<sup>2</sup>**

5 <sup>1</sup> *GET, Université de Toulouse, CNRS, IRD, UPS(Toulouse), France,*

6 <sup>2</sup> *Univ Rennes, CNRS, Géosciences Rennes - UMR 6118, 35000 Rennes, France,*

7 Correspondance to Léopold de Lavaissière (leopold.delavaissiere@gmail.com)

8

9 **ABSTRACT**

10 **The upward propagation of knickpoints in river longitudinal profiles of rivers is commonly**  
11 **related to discrete changes in tectonics, climate or base-level. However, the recognition that some**  
12 **knickpoints may form autogenically, independently of any external perturbation, may challenge**  
13 **these interpretations. We investigate here the genesis and dynamics of such autogenic knickpoints**  
14 **in laboratory experiments at the drainage basin scale, where landscape evolved in response to**  
15 **constant rates of base-level fall and precipitation. Despite this constant forcing, we observe that**  
16 **knickpoints regularly initiate in rivers at the catchments' outlet throughout experiments duration.**  
17 **The upstream propagation rate of knickpoint does not decrease monotonically in relationship with**  
18 **the decrease of their drainage area as predicted by stream-power based models, but it first**  
19 **increases until the mid-part of catchments before decreasing. To investigate the dynamics of the**  
20 **knickpoints, we calculated hydraulic information (water depth, river width, discharge and shear**  
21 **stress) using a hydrodynamic model. We show that heir initiation at the outlet coincides with a**  
22 **fairly abrupt river narrowing entailing an increase in their shear stress. Then, once knickpoints**  
23 **have propagated upward, rivers widen entailing a decrease in shear stress and incision rate,**  
24 **making the river incision lower than the base-level fall rate. This creates an unstable situation**  
25 **which drives the formation of a new knickpoint. The experiments suggest a new cyclic and**

26 **autogenic model of knickpoints generation controlled by river width dynamics regardless of any**  
27 **variations of climate or tectonic rates. This questions an interpretation of landscape**  
28 **records focusing only on climate and tectonic changes without considering autogenic processes.**

29

## 30 **1 Introduction**

31 Knickpoints are discrete zones of steepened bed gradient that are commonly observed in river  
32 longitudinal profiles. Although they occasionally occur due to changes in bedrock properties (e.g. Duvall  
33 et al., 2004), in many cases they are dynamical features that propagate upstream along drainage networks  
34 (Whipple and Tucker, 1999; Kirby and Whipple, 2012; Whittaker and Boulton, 2012). In this last case,  
35 they are commonly considered as formed in response to variations in external forcing such as uplift rate,  
36 sea level or climate (e.g. Crosby and Whipple 2006; Berlin and Anderson, 2007; Kirby and Whipple,  
37 2012; Whittaker and Boulton, 2012; Mitchell and Yanites, 2019) which opens the possibility of using  
38 knickpoints in landscapes to identify such changes. Several studies pointed out however that some  
39 knickpoints could be autogenic, that is to say internally-generated without any variation in boundary  
40 conditions (e.g. Hasbargen and Paola, 2000, 2003; Finnegan and Dietrich, 2011). Understanding how  
41 knickpoints can form autogenically is therefore crucial for retrieving changes in external forcing from  
42 their occurrence in landscapes. Most observations of autogenic knickpoints formation come from  
43 experimental modelling (see for example Paola et al., 2009) their initiation being attributed to  
44 amplification of local instabilities in flume (Scheingross et al., 2019) and drainage basin scale  
45 (Hasbargen and Paola, 2000) experiments. In these latter experiments for example, successive  
46 knickpoints initiated despite constant external forcing (base-level fall and precipitation) throughout the  
47 duration of the runs, even when landscapes were at steady-state on average in terms of sediment flux.  
48 Internal processes may also complexify the propagation of knickpoints as shown in the flume  
49 experiments of Cantelli and Muto (2014) and Grimaud et al. (2016) where a single discrete event of  
50 base-level drop result in the propagation of multiple waves of knickpoints.

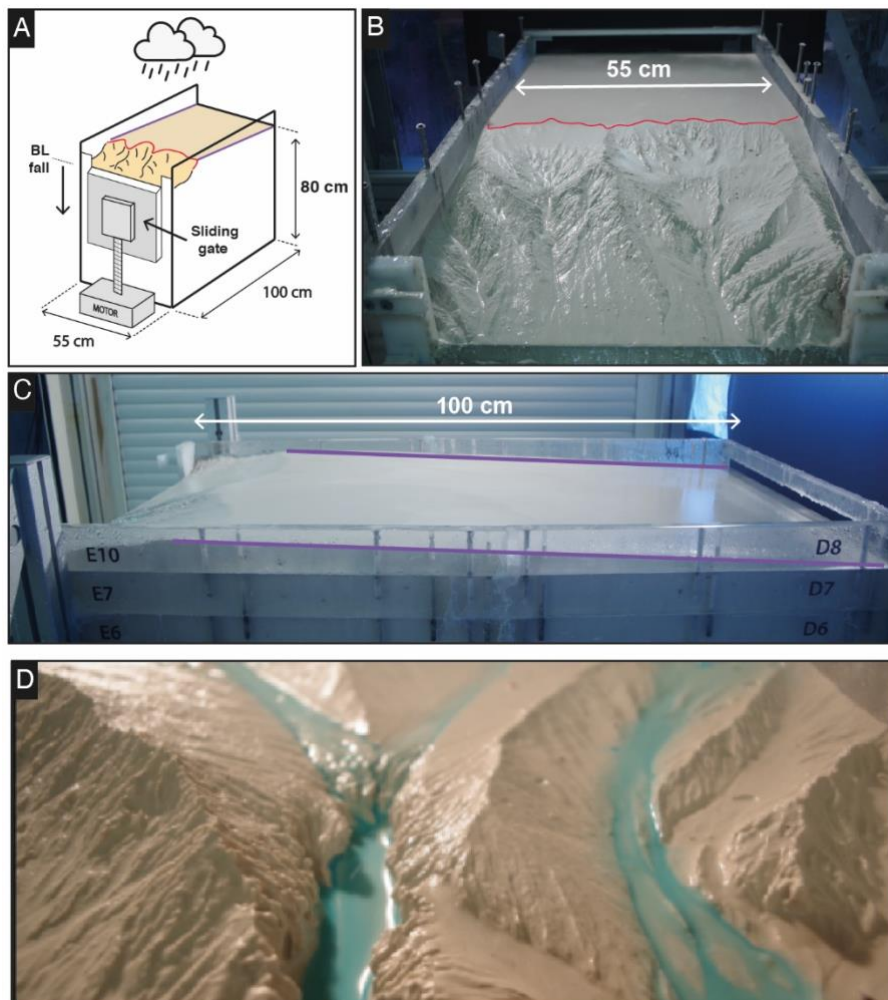
51 In this work, we consider the generation and dynamics of autogenic knickpoints in laboratory-scale  
52 drainage basins experiments forced by constant rate of base-level fall and steady precipitation. Such  
53 landscape experiments have been used successfully to explore how tectonics and climate impact erosion  
54 processes and the evolution of topography under controlled conditions (e.g. Hasbargen and Paola, 2000;  
55 Bonnet and Crave, 2003; Lague et al., 2003; Turowski et al., 2006; Bonnet, 2009; Singh et al., 2015;  
56 Sweeney et al., 2015; Moussirou and Bonnet, 2018). This approach allows for the observation of  
57 complex dynamics that are sometimes difficult to simulate numerically and sheds new light on the way  
58 natural landforms may evolve. Landscape experiments capture the tree-like structure of drainage  
59 networks, the supply of eroded material from hillslopes, and especially their fluctuations, which is a  
60 natural complexity that is not reproduced in flume experiments, for example. The experiments presented  
61 here have been performed using a new setup specifically designed to investigate the evolution of a large,  
62 meter-long, single drainage basin under controlled forcing condition. In previous similar catchment-  
63 scale experiments (Hasbargen and Paola, 2000, 2003; Bigi et al., 2006; Rohais et al., 2012) the outlet  
64 location was pinned to a narrow motor-controlled gate used to simulate base-level fall and which also  
65 set the river width at the outlet. A specificity of our setup here is to use a large gate instead of a narrow  
66 one, allowing experimental rivers to freely evolved downstream, with no constraints on their width. We  
67 report here results from experiments where successive knickpoints initiate near the outlet autogenically  
68 and propagate within drainage basins. The experiments emphasize a new model of autogenic knickpoint  
69 initiation and propagation driven by downstream river width dynamics.

70

## 71 **2 Methods**

72 We present here results from 3 experiments, BL05, BL10 and BL15, performed with different rates of  
73 base level fall, of respectively 5, 10 and 15 mm.h<sup>-1</sup> (Table 1). The facility is a box with dimensions 100  
74 x 55 cm filled with silica paste (Fig. 1; see also Fig. S1 in the Supplemental Material). At its front side,  
75 a sliding gate, 41 cm-wide, drops down at constant rate, acting as the base level. The initial surface  
76 consists on a plane with a counterslope of ~3°, opposite to the base level-side (Fig. 1C). During a run,  
77 runoff-induced erosion occurs in response to steady base level fall and rainfall (mean rainfall rate is of

78 95 mm.h<sup>-1</sup> with a spatial coefficient of variation (standard deviation/mean) of 35%). The mean spatial  
 79 precipitation rate of each experiment is of 95 mm.h<sup>-1</sup>. Incisions initiate at some point along the base level  
 80 and propagate upstream until a complete dissection of the initial surface. Note that the counterslope of  
 81 the initial surface allows to separate the rainfall flux between the base level and the opposite side of the  
 82 device and then to create a water divide (Fig. 1B).



83  
 84 **Figure 1.** Experimental setup. Purple and red lines show respectively the counter-slope of the initial  
 85 topography and the main water divide. (A) Sketch of the erosion box with the sliding gate, 41 cm wide,  
 86 used to drop down the base level (BL). (B), (C) Front and side photographs (experiments BL10 at 525'  
 87 and BL15 at 185'). (D) Photograph of a typical knickpoint studied here.

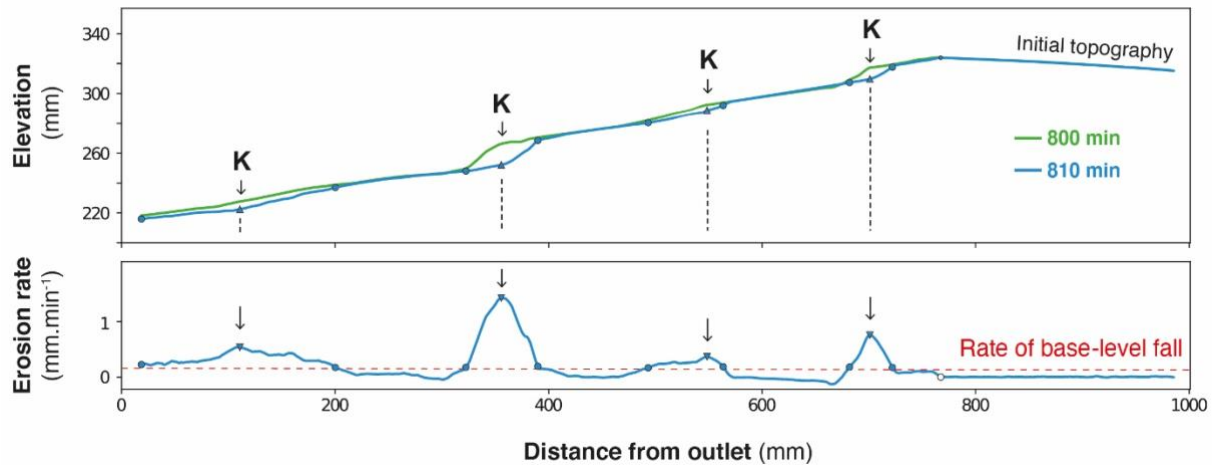
88

89 **Table1.** Parameters of experiments

Experiments	Base Level Fall (mm/h)	Precipitation Rates (mm/h)	Duration Time (min)	Mean Divide Retreat Rates (mm/h)	nDDVmax	Mean Knickpoints Retreat Rates (mm/h)
BL15	15	95	1065	66.3	0.52	183.6 ± 93.8
BL10	10	95	1200	55.7	0.57	164.8 ± 74.8
BL05	5	95	1455	25	0.54	73.1 ± 50

90

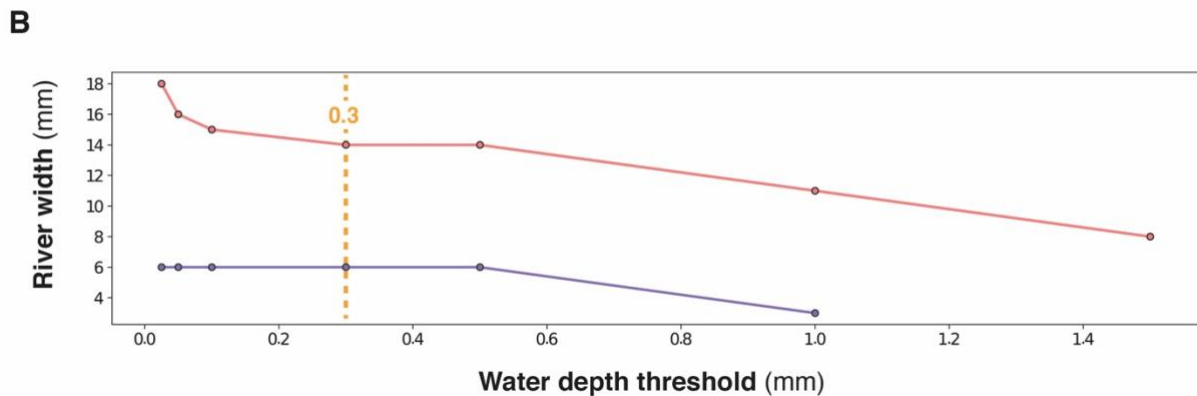
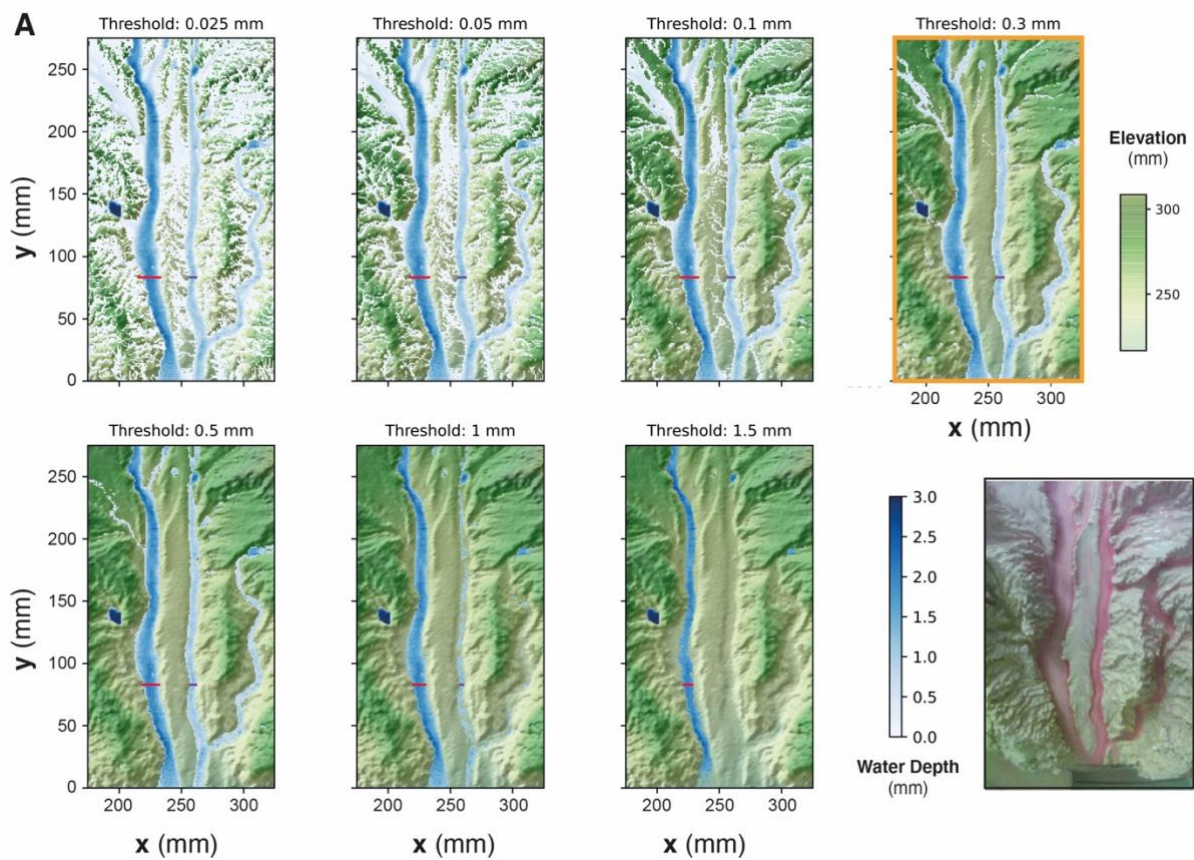
91 Experiments were stopped every 5 min to digitize the topography using a laser sheet and to construct  
92 Digital Elevation Models (DEMs) with a pixel size of 1 mm. Longitudinal profiles and knickpoints were  
93 extracted with a semi-automatic procedure that had to be developed to process the ~200 DEMs per  
94 experiment. For this purpose, we first extracted longitudinal profiles by considering the lowest elevation  
95 on the successive rows of each DEM within a 20 cm-wide swath that included the main river and then  
96 by plotting it against distance down the long axis of the box. This procedure has already been applied  
97 by Baynes et al. (2018) and Tofelde et al. (2019). It may result in a slight overestimation in channel  
98 slope because it does not consider the obliquity of channels within the box in the distance calculation  
99 nor their sinuosity. However, these effects are of minor influence here, because most of channels are  
100 straight and roughly parallel to the long side of the box. In a second step, we computed the elevation  
101 difference between each successive pairs of longitudinal profiles and we identified knickpoints as peaks  
102 in erosion rates with values above the steady erosion amount defined by the rate of base-level fall (Fig.  
103 2). We verified manually that this procedure defines knickpoints correctly by checking the computed  
104 positions on longitudinal profiles. We investigated in particular if the procedure is robust with respect  
105 to the time interval between successive profiles. We found that the record interval of 5 minutes is too  
106 small to produce well-defined erosional peaks, which lead us to identify knickpoint positions from a  
107 time-interval of 10 minutes. Then, we built a first catalogue of knickpoints positions at different times  
108 from which we manually extract the successive positions of each individual knickpoint. We  
109 complemented the database by computing incremental retreat rates of knickpoints from their successive  
110 positions.



111  
 112 **Figure 2.** Graph showing two successive longitudinal profiles of experiment BL10 taken at 10 min  
 113 interval (top) and corresponding erosion rate profile (bottom). Triangles illustrate the position of  
 114 erosional peaks taken as knickpoint position (black arrows). Red dashed line shows the rate of base-  
 115 level fall.

116  
 117 DEMs were also used to compute hydraulic information (water depth, river width, discharge and shear  
 118 stress) using the Floodos hydrodynamic model of Davy et al. (2017; see also Baynes et al. (2018,  
 119 2020) for previous use of Floodos for analyzing laboratory experiments). Floodos is a precipitation-based  
 120 model that calculates the 2D shallow water equations (SWE) without inertia terms, from the routing of  
 121 elementary water volumes on top of topography. We ran Floodos on successive DEMs of experiments  
 122 by considering spatial distribution of precipitation, then generating several output raster products at the  
 123 pixel size, including water depth, unit discharge and bed shear stress that were then used for  
 124 computation of hydrologic parameters (river width, specific discharge and shear stress). The solution  
 125 of the SWE depends on the friction coefficient (C) that depends on water viscosity only for laminar  
 126 flow; its theoretical value is  $\sim 2.5 \times 10^6 \text{ m}^{-1} \cdot \text{s}^{-1}$  at  $10^\circ\text{C}$  (Baynes et al., 2018). To ensure that Floodos  
 127 outputs (e.g. water depth raster maps) calculated using this value are consistent with actual experiment  
 128 hydraulic conditions, we injected dye in the rainfall water during a run to catch the actual extent of  
 129 water flow and make rivers visible. A visual comparison with Floodos results shows a good match  
 130 between model outputs and experimental results (Fig. S2), which validates the numerical method and

131 the expected theoretical friction coefficient  $C$  (Baynes et al., 2018). Given the difficulty to measure the  
 132 mm-scale water depth without perturbing the flow, river widths were extracted from Floodos DEM  
 133 outputs by thresholding the water depth maps, river banks corresponding to sharp variations in water  
 134 depth. The water depth threshold was estimated by trial and error by comparing the rivers extracted  
 135 from the calculation with direct observations on experiments where rainwater was colored by red dye  
 136 (Fig. 3). A good visual agreement was obtained for a threshold value between 0.1 and 0.5 mm, and a  
 137 mid-value of 0.3 mm was then used for determining river widths.  
 138



139

140 **Figure 3.** *Impact of water depth threshold used to delineate river boundaries on estimated river widths,*  
141 *considering a friction coefficient  $C$  of  $2.5 \times 10^6 \text{ m}^{-1} \text{ s}^{-1}$ . A. Map views of water depths (blue colors)*  
142 *superimposed to DEM, for water depths threshold values between 0.025 and 1.5 mm. Red and purple*  
143 *lines show corresponding river widths for two rivers. Photo on the bottom right shows the active river*  
144 *width during the corresponding experimental run, viewed by injecting red dye in the water used to*  
145 *generate the artificial rainfall. B. Corresponding local river widths for the two sections shown by red*  
146 *and purple lines. The use of a low water depth threshold value (e.g. 0.025 mm; top left) leads to the*  
147 *inclusion of large areas of shallow water depth in the “wetted area” considered as rivers and then to*  
148 *unrealistic large rivers in comparison with actual rivers observed in the control run. On the opposite,*  
149 *considering large threshold value (e.g. 1.5 mm) results in narrow rivers, or even in the absence of rivers*  
150 *when maximum computed water depth is lower than this threshold. A threshold value of between 0.1*  
151 *and 0.5 mm shows a good similarity between rivers on water depth map and the control run. Here, a*  
152 *mid-value of 0.3 mm has been chosen for computing river widths.*

153

## 154 **3 Results**

### 155 **3.1 Dynamics of knickpoints retreat**

156 In each experiment, base level fall induces the growth of drainage networks by headward erosion and  
157 the progressive migration of a main water divide (Fig. 4). The migration rate of the divide is constant in  
158 each experiment (Fig. 5 and Table 1), and this value increases from 25 to 66 mm.h<sup>-1</sup> with prescribed rate  
159 of base level fall. The successive longitudinal profiles of the main river investigated in each experiment  
160 (Fig. 6) illustrate the growth of rivers as they propagate within the box. These profiles show alternations  
161 of segments with low and higher slopes, the later defining knickpoints. They regularly initiate at the  
162 outlet throughout the duration of the runs in all experiments and propagate upward until they reach and  
163 merge with the divide, some profiles showing even several knickpoints that retreat simultaneously (Fig.  
164 6). A characteristic of these knickpoints highlighted in Figure 7 (see also Fig. 6) is that they generally  
165 initiate downstream with a gentle slope and gradually steepen as they migrate upstream. Their maximum



166 slope is generally reached when they have propagated to the central part of the profiles (see below).  
167 Then the slope is maintained or slightly decreases during their retreat in the upper segment of the  
168 profiles.

169 The mean retreat velocity of knickpoints varies between experiments from  $73 \pm 50$  to  $183 \pm 94$  mm.h<sup>-1</sup>  
170 (Table 1) and increases as a function of the rate of base-level fall. Data suggest a non-linear relationship  
171 between base-level fall rate and mean retreat velocity of knickpoints, however complementary  
172 experiments would be necessary to constraint this dependency. To investigate the propagation of the  
173 knickpoints, we built space-time diagrams (Fig. 8) by considering the successive alongstream position  
174 of each knickpoint over experimental runtime, as well as the position of the water divide in the box as  
175 already reported in Figure 5. To compare the dynamics of knickpoints within an experiment regardless  
176 of the stage of water divide retreat into the box, the position of knickpoints (distance to outlet, D) has  
177 been normalized to the position of the divide, hereafter referred to as normalized distance to divide  
178 (nDD; nDD=0 at outlet and nDD=1 at the divide; Figure 4). Lines of isovalue of nDD considering an  
179 increment of 0.1 are also shown in the space-time diagrams (Fig. 8). To a first order, the trajectories of  
180 each knickpoint are very comparable within an experiment regardless the stage of retreat of the water  
181 divide and the size of the catchment. Visually for example, in the space-time diagrams there is no  
182 systematic variation in the general slope of the successive knickpoint trajectories over time, as the rivers  
183 expand, that would indicate a change in mean knickpoint velocity in relation to the change in the river  
184 length and catchment size. In detail, an inflection of trajectories is visible for many knickpoints when  
185 they are close to the divide, for  $nDD > \sim 0.8$  (Figure 8), which indicates that they slow down as they  
186 approach the divide. The opposite is observed for some knickpoints when they are close to the outlet,  
187 for  $nDD < \sim 0.2 / 0.3$ , with some trajectories suggesting, on the contrary, an acceleration after their  
188 initiation (Figure 8; see also Fig. 7). These qualitative interpretations are supported by the detail analysis  
189 of retreat velocity data shown in Figure 9. For each experiment, we show in Figure 9A the stack of  
190 successive retreat velocities of each individual knickpoint according to distance nDD. The envelopes  
191 draw a bell-shaped distribution for each experiment, which suggests that retreat velocities are maximum  
192 when knickpoints are located at a mid-distance between the outlet and the divide, for central values of

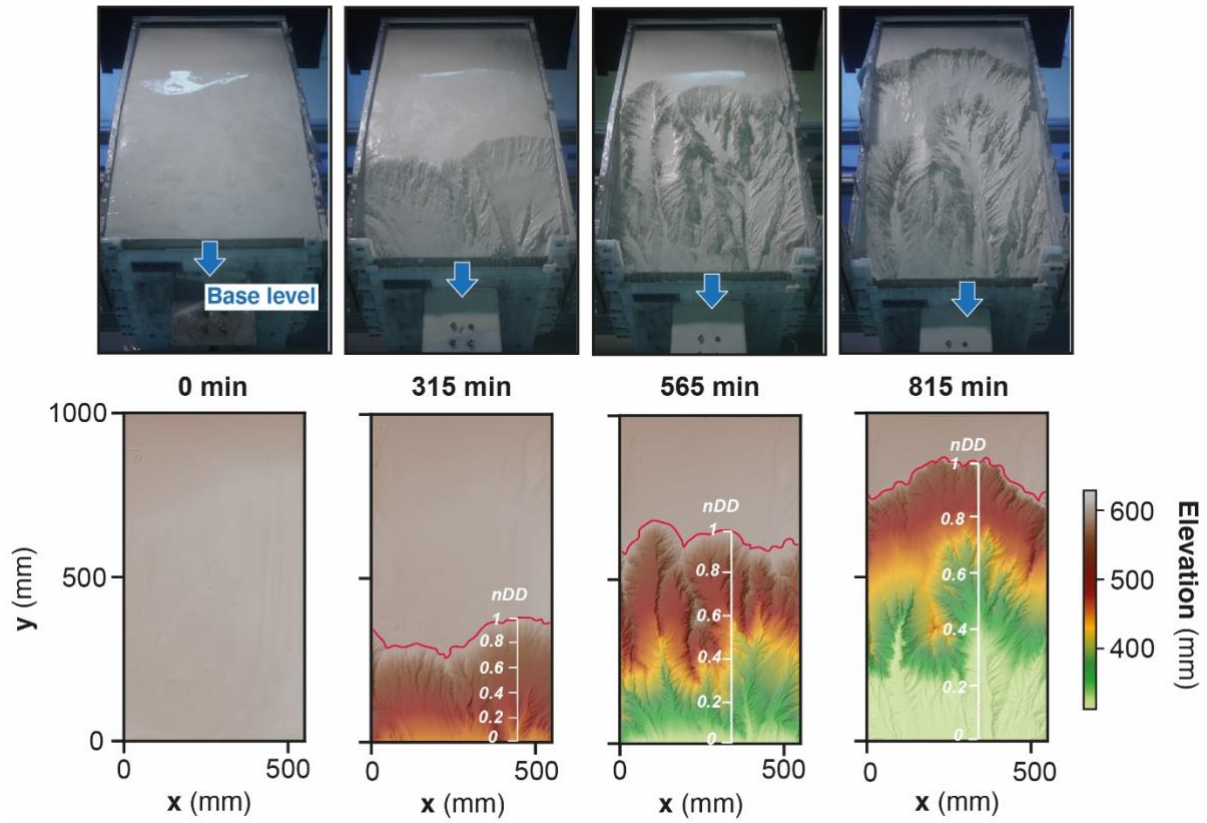
193 nDD, between 0.4 and 0.6. This is supported by summary statistics of retreat velocities at 0.1 intervals  
194 of nDD considering all knickpoints in each experiment (Fig. 9B). Both the mean and median values  
195 show higher rates of upstream propagation when knickpoints are in the central section of rivers in the  
196 three experiments, and conversely lower rates near the outlet ( $nDD < 0.2 / 0.3$ ) where they initiate and  
197 start to propagate and near the divide ( $nDD > 0.8$ ), as suggested by trajectories shown in Figure 8. Note  
198 that because knickpoint retreat rates also depend on the rate of base-level fall, the range of retreat rates  
199 is smaller in experiment with the lower rate of base level fall, BL05, so that their variation with distance  
200 is not as well defined as in both other experiments. However, the mean and median values are also  
201 slightly higher for intermediate distances which suggests that the trends described for the other two  
202 experiments are also valid here. Data from the three experiments indicate that after their initiation near  
203 the outlet, knickpoints first speed up with a maximum in the central part of the catchments before  
204 decelerating near the divide. It is worth noting that this specific trend of knickpoint retreat rates is  
205 observed regardless of the experiment stages and thus whatever the position of the divide in the box.  
206 This applies both to rivers in the early stages of experiments evolution, i.e. when they are small as well  
207 as for very large rivers at the end of experiments. To further characterize this trend, we determined the  
208 position of maximum knickpoint velocity on longitudinal profiles, hereafter  $nDD_{v_{max}}$ , from a second  
209 order polynomial fit (Fig. 9C). This value is very similar between experiments, of 0.52, 0.57 and 0.54  
210 (Table 1).

211

212

213

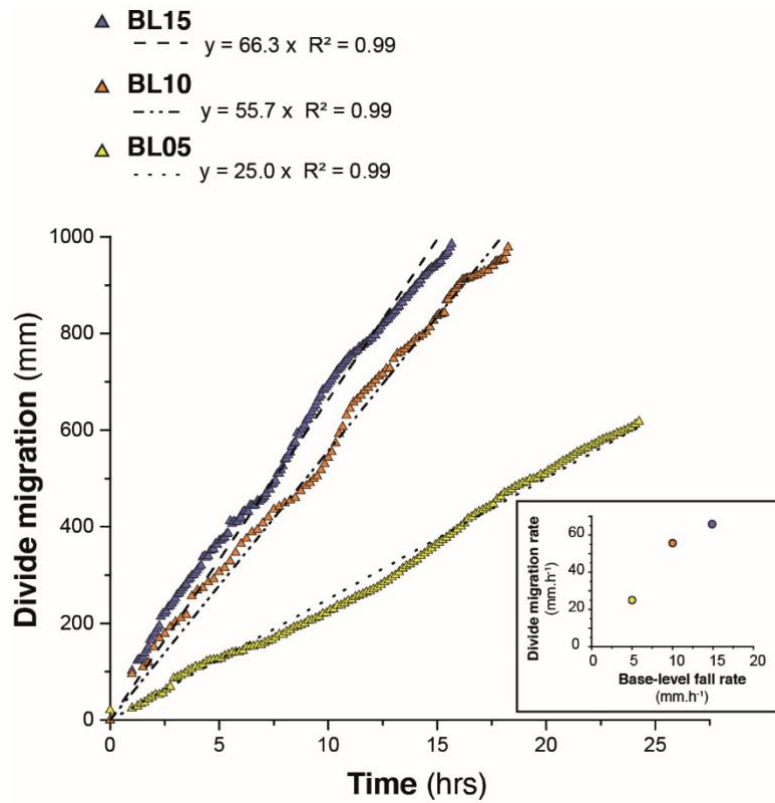
214



215

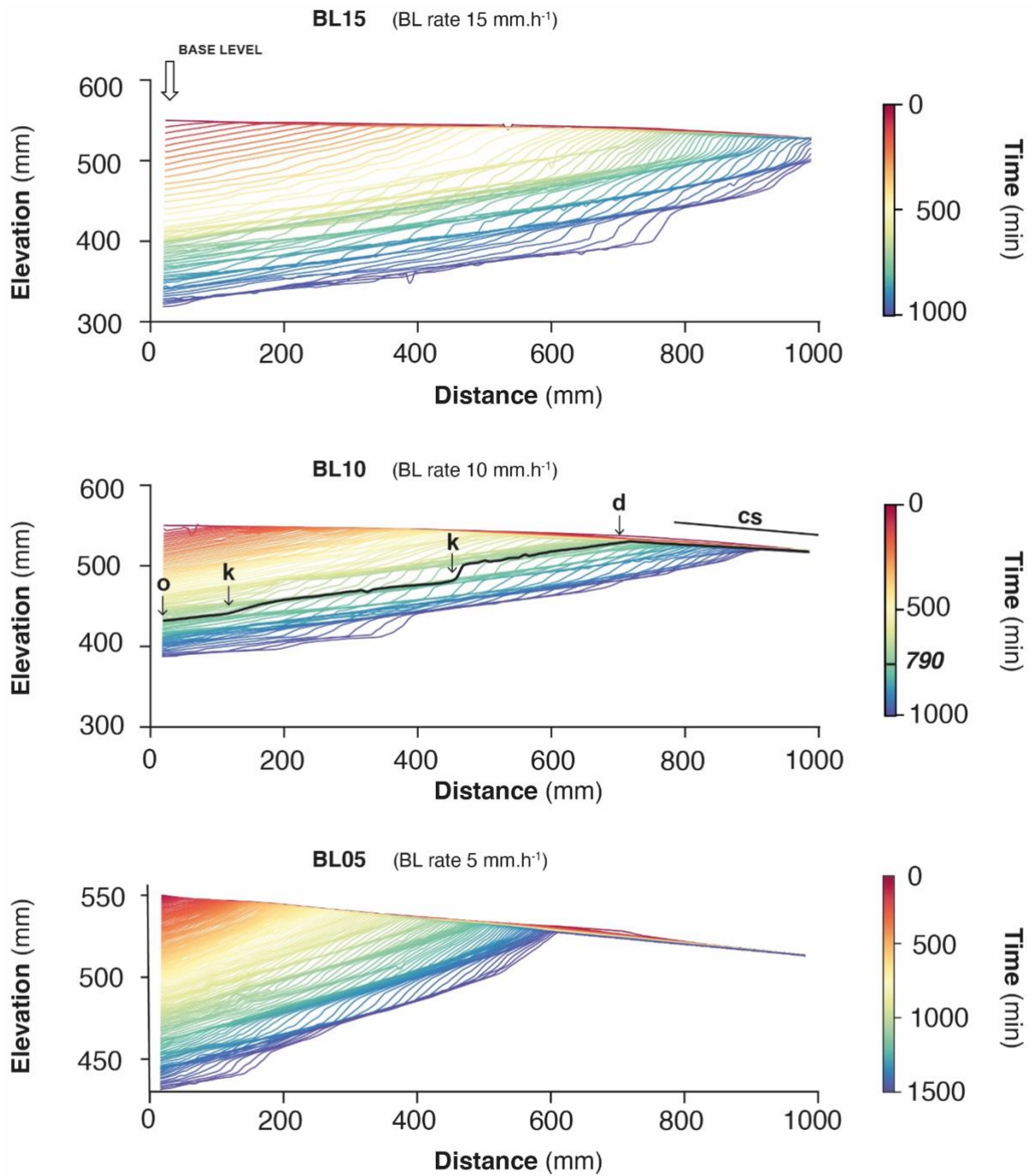
216 **Figure 4.** Photos and corresponding DEMs of experiment BL15 at four runtimes. Note the propagation  
 217 of the divide through the erosion box (red line) and the drop of the sliding gate used for falling base-  
 218 level. The normalized distance to divide ( $nDD$ , see text) used to follow the position of knickpoints during  
 219 runs is shown superimposed to DEMs.

220



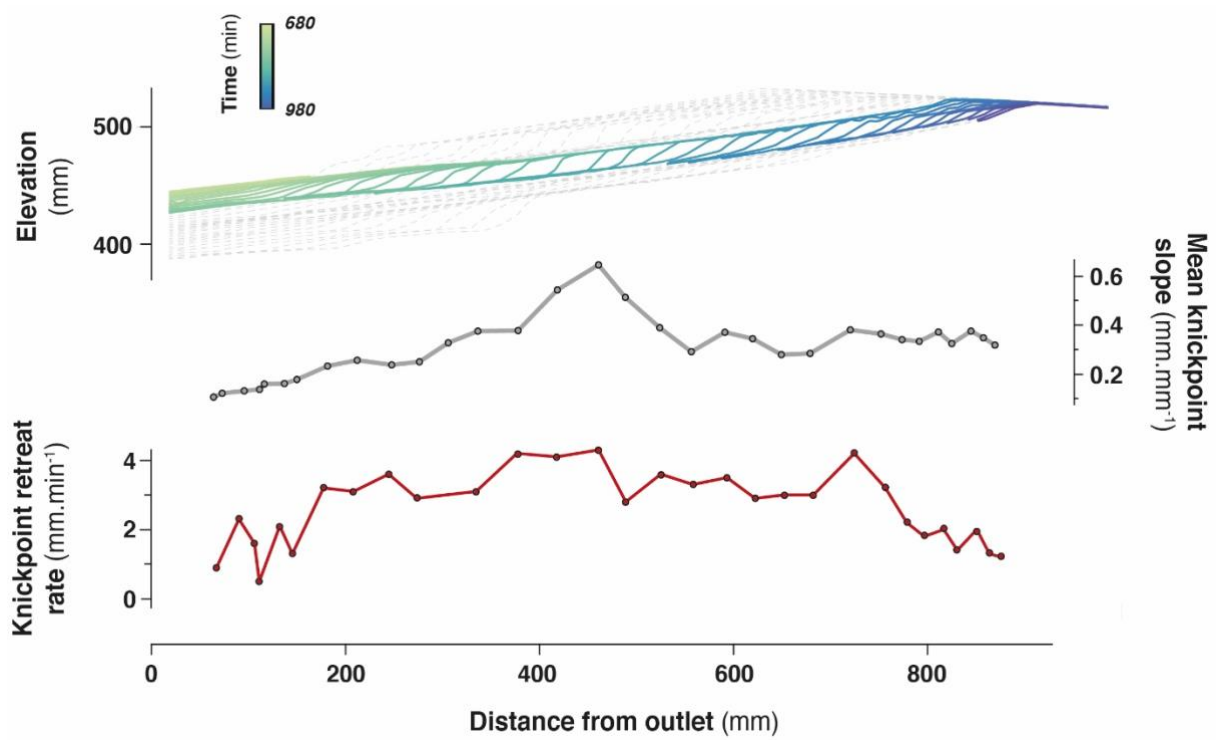
221

222 **Figure 5.** Evolution of the water divide position within the erosion box for the three experiments. The  
 223 inset figure (Bottom right) show the relation between the divide migration rate in the three experiments  
 224 and their related base-level fall rate.



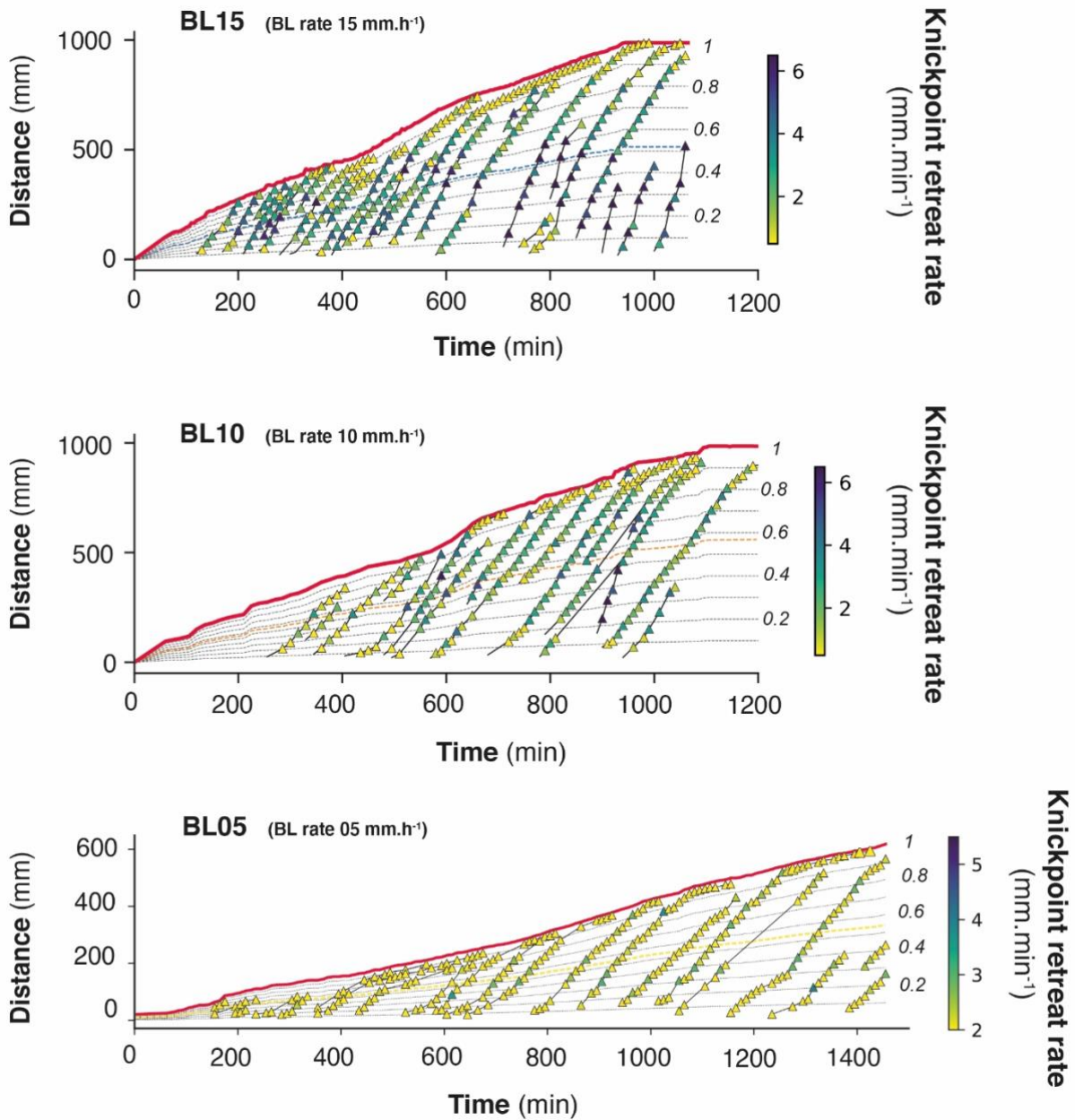
225

226 **Figure 6.** Successive river longitudinal profiles of experiments, shown here every 10 min. Each  
 227 longitudinal profile is colored according to experimental runtime. The sliding gate used to drop the base  
 228 level is to the left. Note the initial counterslope (cs). Black thick line on BL10 is the longitudinal profile  
 229 at  $t=790'$ , illustrating the outlet (o), knickpoints (k), and water divide (d). Note the change of scale for  
 230 experiment BL05.



231

232 **Figure 7.** Detail retreat of an individual knickpoint from experiment BL10 (see also Fig. 6) showing its  
 233 initiation with a gentle slope which subsequently steepen as it migrates upstream (see also Fig. S3). Its  
 234 maximum slope is reached at mid-distance between the outlet and the divide. Its lowest retreat rates are  
 235 observed downstream near the outlet and upstream near the divide.



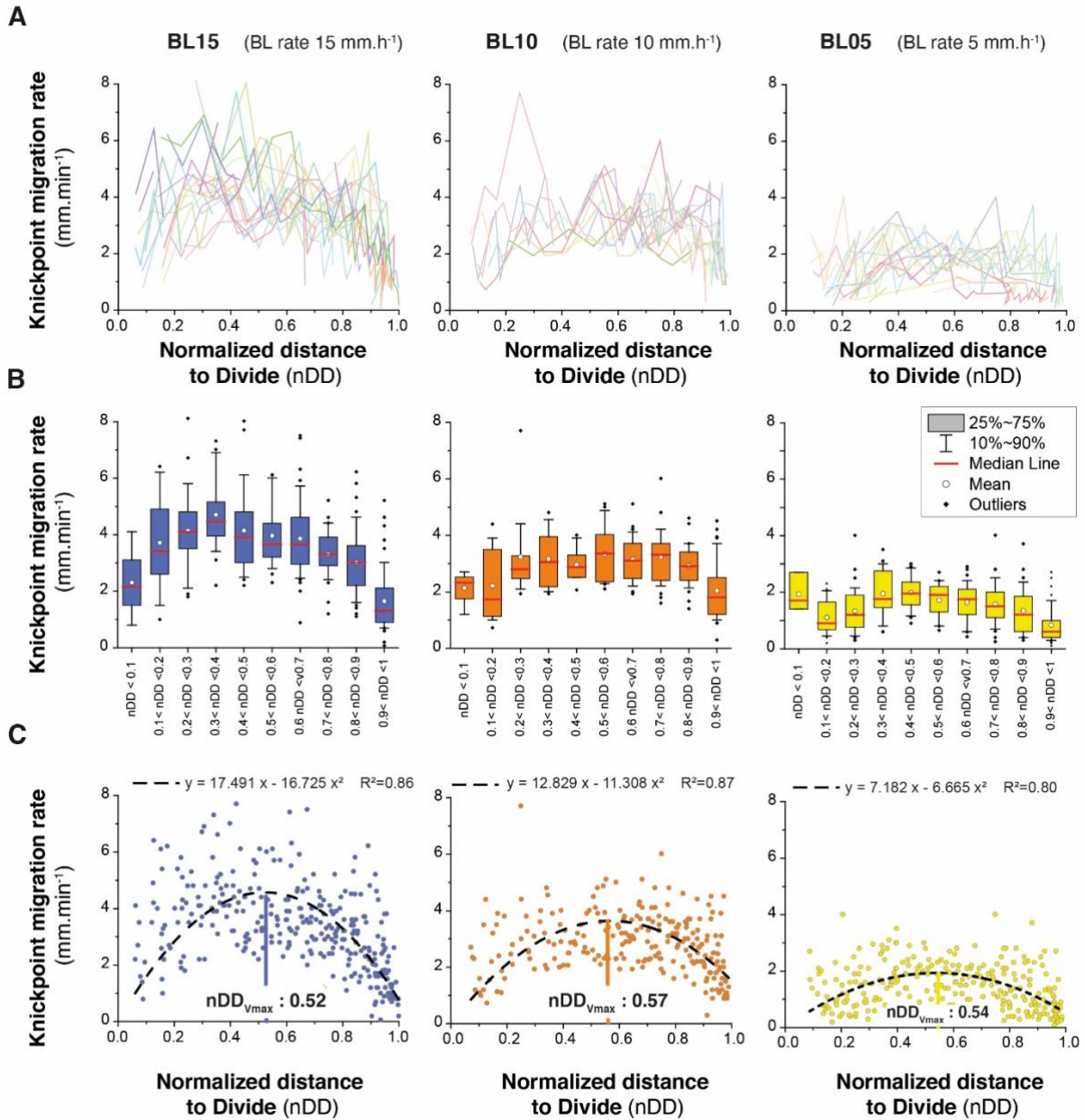
236

237

238 **Figure 8.** Space-time diagrams showing the propagation of the water divide (red line) and successive  
 239 trajectories of knickpoints (triangles). Symbols color shows instant (10 min) knickpoints retreat rate.  
 240 Thin black dashed lines show the normalized distances to divide ( $nDD$ ). Thin colored dashed lines show  
 241  $nDD_{V_{max}}$ , the normalized distance where the highest rate of retreat velocity is deduced from the analysis  
 242 (see text and Figure 9C). Note the change of scale and colorbar for experiment BL05.

243





245

246 **Figure 9.** (A) Knickpoint retreat rates according to the normalized distances to divide (nDD) for each  
 247 knickpoint of experiments. Each color line corresponds to an individual knickpoint of the space-time  
 248 diagram in Fig. 8. (B) Summary statistics of retreat rates for nDD intervals of 0.1. (C) Plot of all  
 249 knickpoints retreat rates for each experiment. Black dashed line shows the second order polynomial fit  
 250 to the data used to define the normalized longitudinal distance of maximum velocity of knickpoints  
 251 ( $nDD_{Vmax}$ ).

252

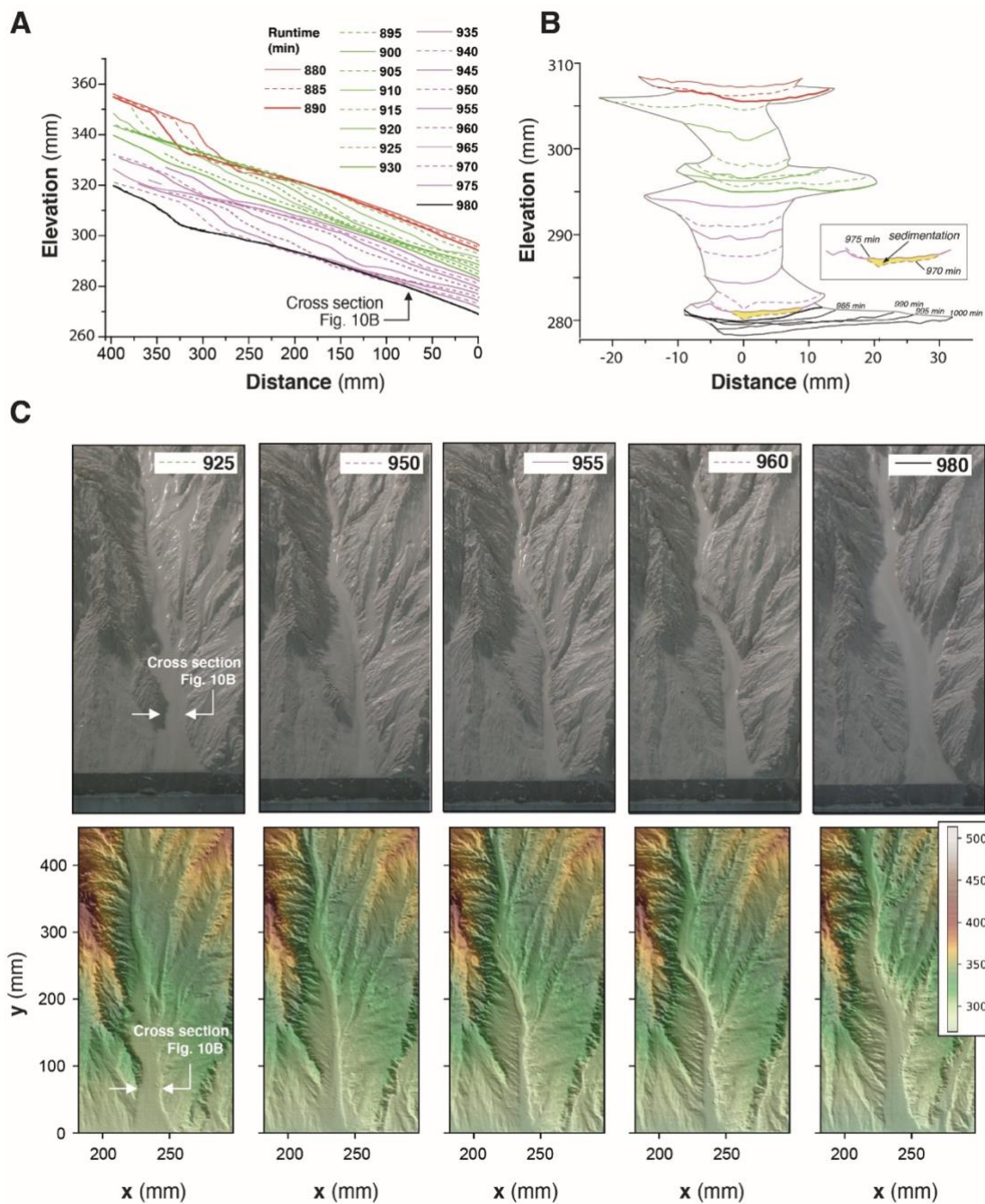


### 253 **3.2 Knickpoints initiation**

254 To illustrate how knickpoints initiated near the outlet, we consider here a 120 minutes-long sequence of  
255 channel evolution in experiment BL15 during which two knickpoints (K1 and K2) successively initiate  
256 and propagate upward (Fig. 10). In addition, we analyzed the history of channel width (Fig. 11A) and  
257 unit water discharge (Fig. 11B) at a cross-section located at 8 cm from the outlet (see location on Fig.  
258 10B). We also present a summary of the statistics of normalized elevation changes (Fig. 11C) and shear  
259 stress (Fig. 11D) for all pixels across the section. The sequence starts with a “standard” profile (i.e., a  
260 typical river profile without any perturbation) at runtimes 880 and 890 min once a previous knickpoint  
261 already propagated, still visible upstream in Figure 10A. The channel is 23 to 25 mm wide (Fig. 10B  
262 and 11A) and the unit discharge is about  $1.5 \cdot 10^6 \text{ mm}^3 \cdot \text{h}^{-1} \cdot \text{mm}^{-1}$ . Erosion in the channel is on average  
263 lower than the base level fall as normalized erosion is  $<1$  for most pixels along the section (Fig. 11C).  
264 Then, the knickpoint K1 initiates at runtime 895' and starts to propagate upstream. At the surveyed  
265 section, the channel first narrows, up to ~15 mm wide at 905 min (~60 % decrease), and then widens  
266 (~25 mm) once the knickpoint has moved upstream of the section, at 910 min (Fig. 10B). The narrowing  
267 phase is naturally associated with an increase of the unit discharge (Fig. 11B) and with an enhanced  
268 erosion well above the base level fall rate, up to 4 times this rate in average at 900 min (Fig. 11 C), with  
269 extremes as high as 8 times the base level rate. Once this knickpoint K1 has retreated, unit discharge  
270 decreases as the channel subsequently widens, to reach a width of 25 cm to 28 cm between 925 and 930  
271 min (Fig. 11A) while a new regular profile, i.e. without any slope break, established at 930 min (Fig.  
272 10A). The normalized erosion across the section decreases below the base level value (Fig. 11C), with  
273 mean erosion rate values of 0.53, 0.36 and 0.76 times below the base level rates between 915 to 925  
274 min. Longitudinally, the profiles stack together downstream of the knickpoint following its retreat from  
275 895 to 925 min (Fig. 10A), which also indicates minor vertical erosion here once the knickpoint has  
276 retreated despite the ongoing base level falling. The second knickpoint (K2) then initiates at 935 min,  
277 propagates upstream in a similar way, and disappears leading to the setting up of a new regular profile  
278 at 980 min (Fig. 10A). Channel narrowing is also observed on the cross-section at the passage of this  
279 second knickpoint with a width that decreases to ~15 mm wide (Fig. 10B and 11A), associated with an

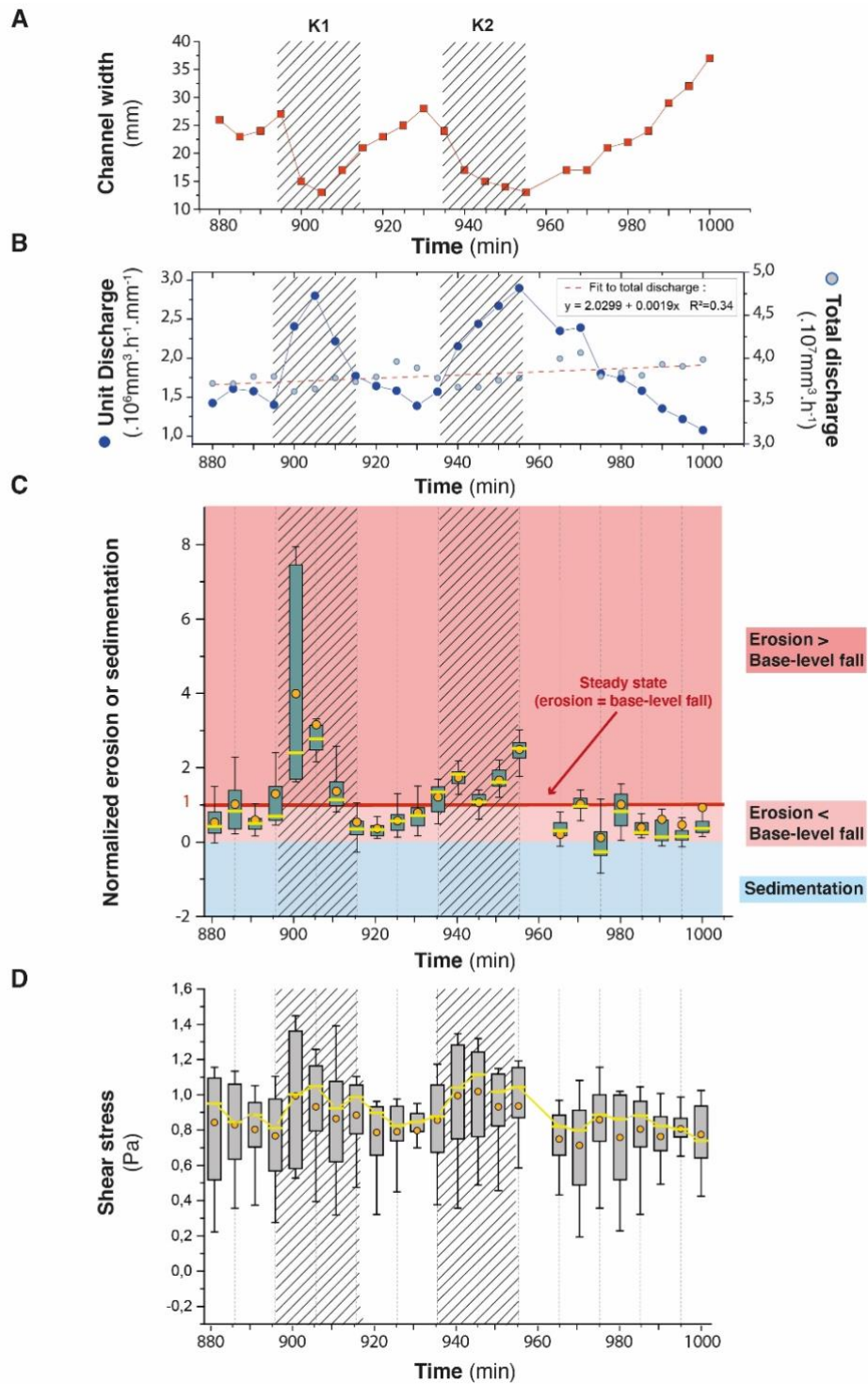
280 increase of the unit discharge and the erosion rate (Fig. 11C). It is followed again by a phase of widening  
281 to reach a width to around 30 / 35 mm once the knickpoint has propagated upstream and by a decreasing  
282 erosion below the base level fall rate (Fig. 11C). Again, the longitudinal profiles stack together  
283 downstream of the knickpoint (Fig. 10A). Note that at 975 min, most of the surveyed section is  
284 undergoing sedimentation (mean normalized erosion rate is 0.1 and median is -0.25: Figures 10B and  
285 11C). The distribution of river bed shear stress along the section is given in the Figure 11D. Despite a  
286 large variability along the section, one can observe a significant increase of the median and maximum  
287 values at the time of the knickpoint passage, both for K1 and K2. Once knickpoints passed, the shear  
288 stresses decrease as the river widens.

289 This sequence illustrates that the rivers are never in equilibrium at the 5 min time-scale, but continuously  
290 oscillate over time between disequilibrium states with periods when channel are too wide to keep pace  
291 with the base level, and periods of knickpoint propagation when the erosion is enhanced to catch up the  
292 base level. The river width is the regulation parameter which allows the river erosion to adapt  
293 by increasing or decreasing the unit discharge. These knickpoints then propagate upward up to the divide  
294 as discussed previously (Fig. 6). The average erosion rate is similar to the baselevel fall rate (0.99) but  
295 it does not correspond to any stable configuration of the river since the erosion rate fluctuates between  
296 smaller and larger values. Knickpoints are by-products of this unsteady dynamics, which are generated  
297 during the phases when the river catches up with its erosion deficit with respect to the base level.



298

299 **Figure 10.** Downstream knickpoints initiation and propagation in a 120 minutes-long sequence of  
 300 experiment BL15 from experimental runtime 880 to 1000 minutes. (A) Sequence of downstream  
 301 longitudinal profiles (5 min time-interval) of the investigated river, corresponding to the sequence  
 302 hydro-geomorphic parameters shown in Figures 11 and 12. Propagation of the first (K1; initiated at  
 303 895') and second (K2; initiated at 935') knickpoints is shown in green and purple colors respectively  
 304 (see text). (B) Time evolution of successive cross-sections of the channel at 80 mm from the outlet. (C)  
 305 Photos and perspective views of DEM at five time-steps.



306

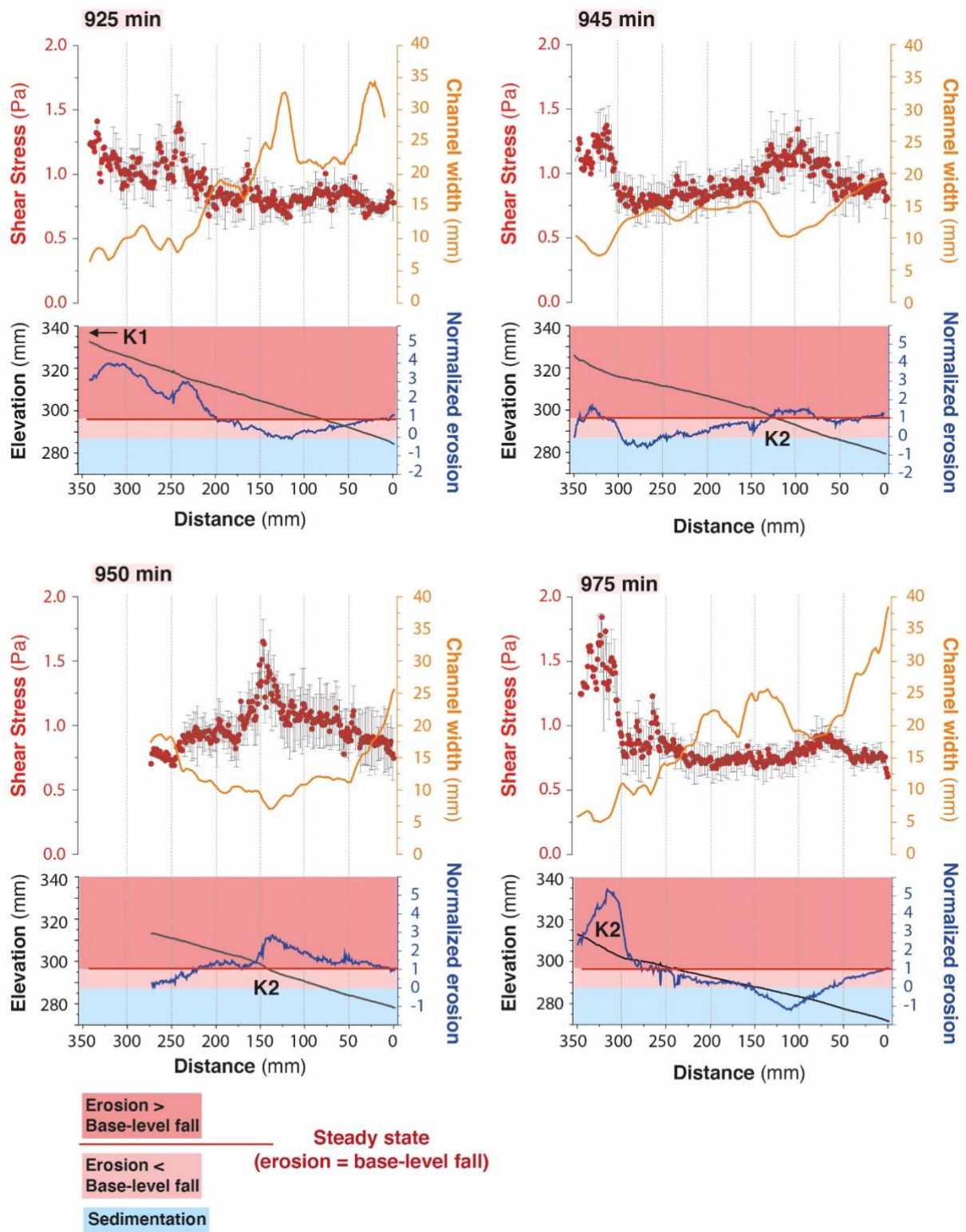
307 **Figure 11.** Time-series (5 min time interval) of river width (A) and unit and total discharge (B) for the  
 308 channel in experiment BL15 shown in Figure 10B. Time-series of box-and-whisker plots of normalized  
 309 erosion or sedimentation (C) and shear stress (D) for all pixels across the section. Orange solid circles  
 310 and yellow lines show the mean and median values respectively. Edges of the boxes indicate the 25th  
 311 and 75<sup>th</sup> percentiles. Note that in C, normalized values of 1 indicate erosion at the same rate than base-

312 *level fall and then steady-state conditions. Values  $> 1$  or  $< 1$  indicate respectively higher and lower*  
313 *erosion rate than BL fall rate. Negative values indicate sedimentation. On all graphs, crosshatched*  
314 *areas indicate the passage of knickpoints K1 and K2.*

315

316 To complement cross-section data, we also illustrate (Fig. 12) how parameters vary longitudinally by  
317 considering four stages, two before (925 min) and after (975 min) the passage of the knickpoint K2 and  
318 two during its retreat (945 and 950 min). Note that at 925 min, the previous knickpoint (K1) has just  
319 passed upstream the investigated profile and is responsible for the enhanced normalized erosion and  
320 increased shear stress upstream between distance 200 to 350 mm. Similarly, at 975 min the second  
321 knickpoint (K2) is still in the upstream part of the profile between distance 300 to 350 mm. We also  
322 reported the longitudinal variations in river width, shear stress and normalized erosion along the profiles  
323 (Fig. 12). At runtimes 925 and 975 min, before and after the passage of knickpoint K2, erosion is below  
324 the base level rate along all the profiles down the knickpoints, with even localized sedimentation at 975  
325 min between 50 and ~150 mm. These sections are characterized by low shear stress values, being  
326 between 0.5 and 1 and by rivers that widen downward (around 0.7 mm/cm). On the opposite, during the  
327 passage of knickpoint K2, at runtimes 945 and 950 min, mean shear stress increases locally at the  
328 knickpoint location, being  $> 1$  and the normalized erosion overpasses the base level rate there. These  
329 knickpoint segments are characterized by a narrowing of the rivers as already shown previously. The  
330 data illustrate that erosion mainly occurs during periods of knickpoint retreat though a combination of  
331 local steepening of the profile and narrowing of the river, resulting in an increased shear stress. On the  
332 opposite, once a knickpoint has propagated and between the passage of two successive knickpoints,  
333 erosion decreases significantly and does not longer compensate the base level fall. These periods of  
334 defeated erosion are characterized by low bed shear stress values in wide rivers, that widen downward.





335

336 **Figure 12.** Longitudinal trends of hydro-geomorphic parameters in experiment BL15 at runtimes 925,  
 337 945, 950 and 975 min (see text for comments). K1 and K2: first and second knickpoints discussed in the  
 338 text (see also Fig. 10A).

## 339 **4 Discussion**

### 340 **4.1 Autogenic knickpoints**

341 Our experiments illustrate the generation and retreat of successive knickpoint waves that traveled across  
342 the landscape during the growth of drainage networks. They formed throughout the duration of  
343 experiments regardless of the steadiness of the precipitation and base level fall rates and of the  
344 homogeneity of the eroded material. These knickpoints were autogenically generated (Hasbargen and  
345 Paola, 2000), arising only from internal geomorphic adjustments within the catchments rather than from  
346 variation in external forcing. Our observations appear very similar to those of Hasbargen and Paola  
347 (2000, 2003) and Bigi et al. (2006) who also reported the generation of successive autogenic knickpoints  
348 in landscape experiments evolving under steady forcing (rainfall and base level fall rate) throughout the  
349 duration of the runs. Unlike our experiments, which mainly consider the growth phase of drainage  
350 networks, experiments reported in Hasbargen and Paola (2000, 2003) and Bigi et al. (2006) considered  
351 the propagation of knickpoints after the phase of network growth, while their system was at steady-state  
352 on average (mean catchment erosion rate equals to base level rate). Then, given that the size of their  
353 experimental catchment was steady over time and given the steady rainfall rate, they were able to rule  
354 out variations of water discharge over time as a main driver for the generation of their knickpoints. On  
355 the opposite, in our experiments the size of catchments continuously increased over time, and thus the  
356 water discharge. However, this does not appear as a key factor controlling knickpoints initiation for  
357 several reasons. First, as we already mentioned, knickpoints arose at all stages of network growth and  
358 divide retreat, for both small and large rivers (Fig. 8), and thus whatever the range of water discharge at  
359 outlet. Second, the migration of the water divide related to drainage network growth occurred steadily  
360 and roughly at a constant rate during the experiments (see Figures 5 and 8), as well as the size of the  
361 catchments and the related increase in water discharge. Then, we can rule out abrupt variations in  
362 discharge as the driving mechanism for knickpoint initiation. Last, knickpoint initiations occurred at a  
363 higher frequency than the increase in water discharge that resulted from catchment expansion and divide  
364 migration. For example, in addition to unit discharge, we also reported on Figure 11B the variation in  
365 total discharge during the 120 min-long sequence of knickpoint initiation discussed previously. The total

366 discharge rose from  $3.7 \cdot 10^7$  to  $4.0 \cdot 10^7 \text{ mm}^3 \cdot \text{h}^{-1}$  in 120 minutes representing a  $\sim 8\%$  increase, which is  
367 relatively low compared to the  $\sim 100\%$  increase of unit discharge during the passage of a knickpoint.  
368 For all these reasons we conclude that the change in catchment size was not the main driver of successive  
369 knickpoints initiation in our experiments, which occurred at a higher frequency.

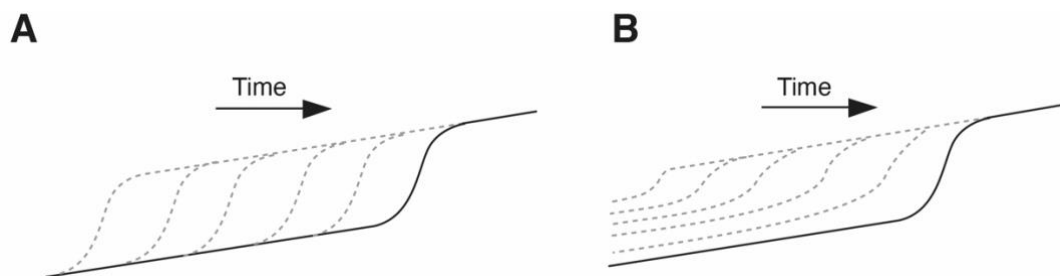
#### 370 **4.2 Processes controlling knickpoints initiation and propagation**

371 Given that the initiation of successive knickpoints was not related to changes in external factors and  
372 catchment size over time, we consider internal geomorphic processes as driving mechanisms. The  
373 detailed sequence of knickpoints initiation and propagation discussed above shows enhanced incision  
374 above the rate of base level fall during the periods of knickpoints propagation. This occurred through  
375 local steepening of the longitudinal profile and narrowing of the river, these two factors leading to an  
376 increase in unit discharge and bed shear stress along the knickpoints. Several studies already  
377 documented how steepening and narrowing act together for increasing river incision rate (e.g. Lavé and  
378 Avouac, 2001; Duvall et al., 2004; Whittaker et al., 2007; Cook et al., 2013), which is what we also  
379 document here. The novelty in our finding here, however, lies in the phase of post-knickpoint retreat.  
380 Actually, immediately after the retreat of a knickpoint, we show that erosion is inhibited downstream  
381 and rivers no longer incised despite the ongoing base level fall, until the passage of a new knickpoint.  
382 Although only illustrated in the sequence detailed previously (Figs. 10 to 12), this was a general behavior  
383 that concerned the three experiments and their whole longitudinal profile, not only their downstream  
384 part as in this sequence. Actually, this systematic decrease in erosion downstream of the knickpoints is  
385 inherent to the geometry of the stacks of all successive longitudinal profiles of each experiment (Fig. 6).  
386 In most cases, profiles downstream of retreating knickpoints stack on top of each other, as illustrated  
387 schematically on Figure 13A, which indicates minor or no erosion downstream of the knickpoints until  
388 the passage of a new one. In the case of continuous adjustment of rivers to base level fall downstream  
389 of the knickpoints, the geometry of profiles should rather show a pattern as illustrated in Figure 13B.  
390 The pattern of profiles evolution over time documented here is usually observed following incremental  
391 drops in base level (Finnegan, 2013; Grimaud et al., 2016) and to our best knowledge this is the first  
392 time here that such geometry is documented in the case of a continuous base level fall. This particular

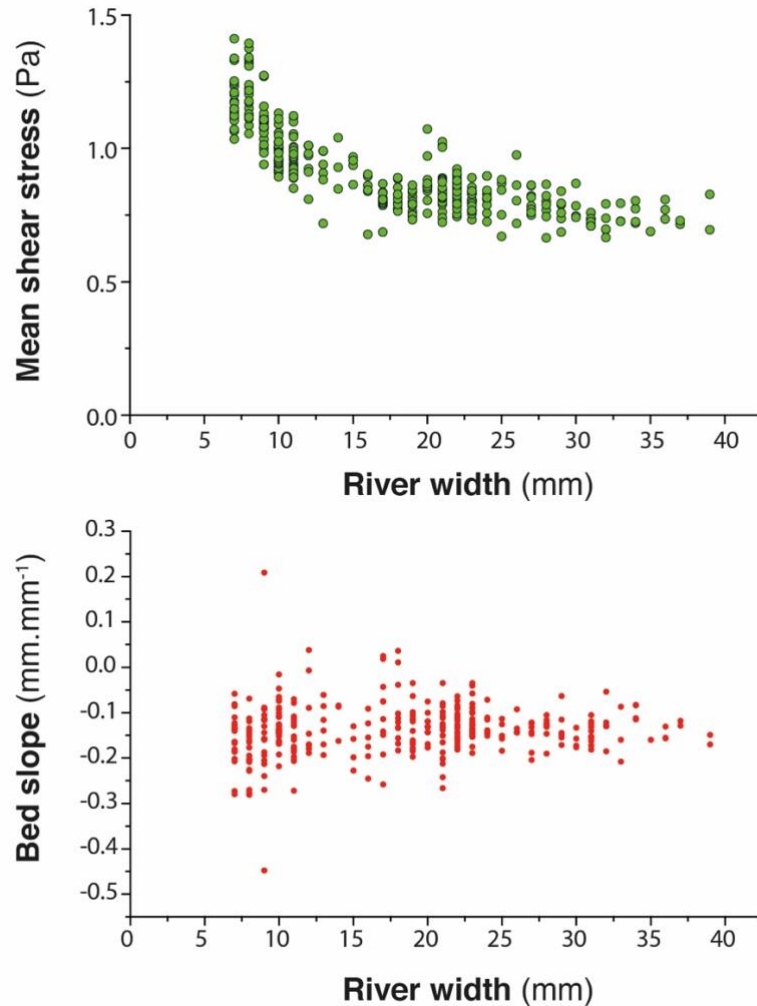


393 pattern is explained by the decrease in erosion rate downstream of the retreating knickpoints which  
394 finally acts as if the base level was not falling continuously at a constant rate but dropped regularly step-  
395 by-step. Therefore, understanding the systematic occurrence of successive knickpoints in our  
396 experiments requires to understand why erosion rate dropped downstream of knickpoints, following  
397 their retreat. After the passage of knickpoints, we systematically observe a widening of the rivers, as  
398 also documented in natural systems (e.g. Cook et al., 2014; Zavala-Ortiz et al., 2021) and a decrease in  
399 the bed shear stress. Because an increase in channel width over time inevitably reduces the bed shear  
400 stress if discharge and river gradient remain constant (Fuller et al., 2016), we propose that widening was  
401 the main factor responsible for the decrease in shear stress and erosion rate after the passage of a  
402 knickpoint, and then for the occurrence of the successive autogenic knickpoints. Demonstrating the sole  
403 effect of river width on bed shear stress and erosion rate is complicated by covariations of these factors  
404 with river slope and variations of discharge related to connection of tributaries. This can be illustrated  
405 however on the basis of the sequence considered previously, particularly at runtime 925 min between  
406 the passage of the two successive knickpoints K1 and K2 (Figs. 10 and 12). At that time, the profile of  
407 the river here had a roughly constant slope (Fig. 14), without any slope break and no major tributary  
408 connected (Fig. 10) that could have significantly changed the water discharge. As illustrated in Figure  
409 12, this river segment was characterized by widening and decreasing shear stress downward despite  
410 constant slope and total discharge. Then, this example illustrates a decrease in shear stress that was only  
411 the result of the widening of the river downward (Fig. 14), which supports the hypothesis that defeated  
412 erosion downstream of the propagating knickpoints was mainly due to the widening dynamics of the  
413 experimental rivers.

414



415 **Figure 13.** Sketches illustrating the difference in the geometry of successive longitudinal profiles  
416 following the retreat of a knickpoint depending on whether fluvial incision is inhibited (A) or not (B)  
417 downstream of the retreating knickpoint with respect to the continuously falling base level.



418

419 **Figure 14.** Top: river bed shear stress according to river width in the downstream section, 40 cm-long,  
420 of experiment BL15 at runtime 925 (see also Fig. 12). Bottom: corresponding slope of the river bed.

421 Incision of rivers in our experiments is fundamentally discontinuous despite continuous forcing and we  
422 highlight downstream river width dynamics, in particular river widening, as a main cause of instability.

423 We show that once knickpoints have retreated, unit discharge, shear stress and incision rate all decrease  
424 downstream while the rivers widen, resulting in a state where incision no longer counterbalance the  
425 base-level fall. This results in an unstable situation that ends up with the initiation and propagation of a  
426 new knickpoint and a new sequence of width narrowing, increasing shear stress and incision rate,

427 allowing the river to recover from the incision delay accumulated during the previous widening period.  
428 Further work is required to understand the mechanisms responsible for lateral channel erosion in our  
429 experiments, which is a key ingredient for understanding river mobility and widening. Several field (e.g.  
430 Hartshorn et al., 2002; Turowski et al., 2008; Fuller et al., 2009), experimental (e.g. Wickert et al., 2013;  
431 Bufe et al., 2016; Fuller et al., 2016; Baynes et al., 2020) and numerical (e.g. Turowski et al., 2007;  
432 Lague, 2010; Langston and Tucker, 2018; Li et al., 2021) studies have demonstrated that high sediment  
433 flux relative to transport capacity promotes increased lateral channel erosion. Most of these studies  
434 highlight the role of cover effect, the protection of the river bed by transient deposition of sediments on  
435 the river bed (Sklar and Dietrich, 2001; Turowski et al., 2007, 2008; Lague, 2010; Baynes et al., 2020;  
436 Li et al., 2021), as a main factor promoting lateral erosion in high sediment flux settings. Other studies  
437 show that by modifying the bed roughness, sediment deposition may deflect the flow, which also  
438 promotes lateral erosion and widening (Finnegan et al., 2007; Fuller et al., 2016). Contrary to  
439 experimental devices specifically designed to address these issues, large flumes in particular (e.g.  
440 Finnegan et al., 2007; Fuller et al., 2016), direct observation on actual processes that drive lateral erosion  
441 in our experiments is made difficult by the small size of the topographic features, the depth of rivers  
442 being of millimeter scale, and by the low grain size of the material used. Opacity due to the generation  
443 of the artificial rainfall also considerably limits direct observation during the runs. Despite these  
444 limitations, data suggest that lateral erosion and river widening in our experiments is also related to  
445 increase in sediment flux. We show actually that knickpoints are location of enhanced erosion well  
446 above the rate of base level fall. We document for example mean erosion rates greater than 5 times the  
447 base level fall rate, with extreme values up to a factor of 8 locally (Fig. 11 and 12). Downstream, where  
448 rivers widen, we observe that the general decrease in erosion rate is also associated with local deposition  
449 in some parts of the channels (for example at runtime 915 min in Figure 11 or 975 min in Figures 10 to  
450 12). We then hypothesize that lateral erosion and widening are due in part to the increase sediment flux  
451 related to enhanced erosion on knickpoints. Further work is needed to test this hypothesis, for example  
452 by investigating in detail spatio-temporal variations in erosion and sedimentation during width  
453 widening.

454 Further work is also needed to better understand how knickpoints initiate after the phases of widening,  
455 in particular for determining whether river narrowing drives the formation of the knickpoints (e.g. Amos  
456 and Burbank, 2007) or whether narrowing is a consequence of steepening (e.g. Finnegan et al., 2005).  
457 Some studies that investigated the rivers response to increased uplift rate show that narrowing alone, at  
458 constant river gradient, can allow rivers to increase their incision rate (Lavé and Avouac, 2001; Duvall  
459 et al., 2004; Amos et al., 2007). In this context, Amos et al. (2007) propose a model in which the river  
460 response to an increase in uplift rate first involves width narrowing, with the increase in slope and  
461 formation of a knickpoint occurring only in a second stage, if the increase in incision induced by  
462 narrowing is not sufficient to counteract the uplift rate. In our experiments here, we suggest that channel  
463 narrowing predates, and in fact enables, the steepening of the profile in the initial stages of knickpoints  
464 formation. Indeed, we observe that the transition from a wide to a narrow channel occurs very quickly,  
465 at a smaller time scale than the time interval between two successive digitization of the experiments (5  
466 min), and the knickpoints that form then have a very gentle slope, which then amplifies as they migrate  
467 upstream (Fig. 7). This suggests that it is not the steepening that drives river narrowing but on the  
468 contrary that narrowing is essential for knickpoints to initiate. Further work would also be needed to  
469 verify this hypothesis, in particular with additional experiments with much higher frequency of data  
470 acquisition to capture these changes in much more detail.

### 471 **4.3 Implications**

472 Knickpoints in river longitudinal profiles are commonly related to variations in tectonics or climate  
473 through their influence on base level and/or sediment supply (e.g. Whipple and Tucker, 1999; Crosby  
474 and Whipple, 2006; Kirby and Whipple, 2012; Whittaker and Boulton, 2012) and are then used to  
475 highlight such changes when interpreting their occurrence in natural systems. The recognition here that  
476 knickpoints may be generated autogenically due to cycles of river widening and narrowing is then of  
477 first importance for retrieving information on tectonics and climate from their record in landscapes in  
478 the form of knickpoints. Finding criteria that could be used in the analysis of natural systems to  
479 differentiate these autocyclic knickpoints from those formed in response to tectonics or climate would  
480 be an important step in the continuation of this work. A specificity of knickpoints in our experiments is

481 to initiate downstream with a gentle slope, which then amplifies in the early stages of migration, and as  
482 a hypothesis we suggest that this may be characteristic of their autogenic formation following the  
483 mechanism described here. Being able to recognize these autogenic knickpoints would also be important  
484 for studies that investigate knickpoints propagation (e.g. Crosby and Whipple 2006; Berlin and  
485 Anderson, 2007; Schwanghart and Scherler, 2020) because knickpoints in our experiments are  
486 characterized by an upward dynamic of retreat that is not conventional. According to stream-power  
487 based celerity models, these studies consider that the upstream propagation rate of knickpoints depends  
488 inversely on drainage area (a proxy for discharge; Crosby and Whipple 2006; Berlin and Anderson,  
489 2007), implying a monotonous decrease of their retreat rate as they propagate upstream due to the  
490 progressive reduction of drainage area and water discharge. This property is used for example to invert  
491 their present location for dating the external perturbation responsible for their formation (Crosby and  
492 Whipple 2006; Berlin and Anderson, 2007). Here, knickpoints in our experiments first accelerate during  
493 their initial stages of propagation before decelerating in a second time as they approach the divide  
494 (Fig.9). Only this later phase of decreasing knickpoint velocity in the upstream part of rivers (for  
495 normalized distance  $NDD > nDD_{v_{max}}$ : Fig. 9) is consistent with predictions from stream-power based  
496 celerity models (see Fig. S4 in the Supplemental Material). On the opposite, a sole control by drainage  
497 area and discharge cannot explain the increase in velocity observed in the downstream sections (for  
498  $NDD < nDD_{v_{max}}$ : Fig. 9), which implies an additional controlling factor. We suggest that this specific  
499 mode of retreat downstream is related to the progressive steepening of the knickpoints (Fig. 7) rather  
500 than to a purely hydrologic control. Deciphering the respective roles of slope and discharge in the retreat  
501 dynamics documented would require further in-depth analysis, particularly during the early stages of  
502 initiation and propagation which appear to be specific to the autogenic mechanism defined here.

503 We show that the formation of knickpoints in our experiments is closely related to periods of decreasing  
504 erosion rate as the rivers widen, counterbalanced by increasing rate greater than the rate of base level  
505 fall as the rivers narrow and knickpoints form. Thus, the sequential evolution of longitudinal profiles is  
506 more consistent with the geometry that would be observed if the system was forced by discrete drop of  
507 the base level, rather than by a continuous base level drop as it is actually the case. We did not measure

508 the sediment flux at the output of our models, but we can assume that it would be characterized by  
509 fluctuations controlled by the frequency of knickpoint initiation, superimposed on a longer-term  
510 increasing trend related to the growth of drainage networks. Some sediment outflux fluctuations were  
511 actually measured by Hasbargen and Paola (2000) in their experiments and interpreted as the  
512 consequence of knickpoint propagation. This study and our work illustrate that fluctuations in sediment  
513 flux can be observed at catchments outlet despite constant forcing parameters, when autocyclic  
514 knickpoints are generated in river systems.

515 By performing such exploratory experiments, we do not pretend to reproduce natural landscapes in the  
516 laboratory because of important scaling issues (see Paola et al., 2009 for an extensive reflection on this  
517 matter) but rather to highlight and document complex system behaviors under controlled conditions that  
518 could provoke further investigations. Our findings support ongoing investigations that aim in better  
519 understanding the links between lateral erosion, channel geometry and valley width which is an issue  
520 that is emerging in the last years (e.g. Turowski, 2018; Croissant et al., 2019; Langston and Tucker,  
521 2019; Baynes et al., 2020; Zavala-Ortiz et al., 2021). A perspective to our work would be to investigate  
522 the mechanism of knickpoints generation driven by river width variations and the conditions that lead  
523 to their formation using landscape evolution models that incorporate lateral erosion and a dynamic river  
524 width (e.g. Davy et al., 2017; Carretier et al., 2018; Langston and Tucker, 2019). Simulations of  
525 Langston and Tucker (2019) highlight the role of bedrock erodibility as an important factor controlling  
526 lateral migration of rivers and the width of valleys, an issue that has not been investigated here given  
527 the similarity of the eroded materials in our experiments here. This study also confirms the assumption  
528 of Hancock and Anderson (2002) that lateral erosion and widening occurs preferentially in contexts of  
529 low incision rate, *i.e.* in domains with low uplift rate. This is likely in such contexts that the new mode  
530 of autogenic knickpoints formation driven by river width dynamics that we define in this study should  
531 apply.

## 532 **5 Conclusions**

533 Knickpoints in the longitudinal profile of rivers are commonly considered as incisional waves that  
534 propagate upstream through landscapes in response to changes in tectonics, climate or base-level. Based

535 on results from a set of laboratory experiments at the drainage basin scale that simulate the growth of  
536 drainage networks in response to constant base level fall and rainfall, we show that knickpoints also  
537 form autogenically, independently of any variations in these external forcing factors. In all experiments,  
538 successive knickpoints initiate and propagate upward throughout the duration of the experimental runs,  
539 regardless of the rate of base level fall applied and of the size of the rivers, as the catchments expand.  
540 Thanks to the computation of hydraulic information (water depth, river width, discharge and shear  
541 stress) using a hydrodynamic model, we show that the formation of knickpoints is driven by variations  
542 in river width at the outlet of catchments and we highlight width widening as a main cause of instability  
543 leading to knickpoint formation. Widening actually entails a decrease in shear stress and an incision rate  
544 lower than the rate of base level fall, resulting in an unstable situation that ends up with a sequence of  
545 width narrowing, increasing shear stress and incision rate as a knickpoint initiates. Rivers in our  
546 experiments thus evolve following sequences of width widening and narrowing that drive the initiation  
547 and propagation of successive knickpoints. As a result, incision is fundamentally discontinuous over  
548 time despite continuous forcing. It occurs during discrete events of knickpoint propagation that allows  
549 the rivers to recover from the incision delay accumulated during widening periods.

550

551 **Author contributions.** SB designed the experimental device. LdL, SB and AG built the experimental  
552 setup and carried out the experiments. LdL analyzed the data with the help of SB and PhD. All authors  
553 discussed the data. LdL and SB wrote the manuscript with input from AG and PhD.

554

555 **Acknowledgements.** This work was supported by ORANO-Malvesi and CNRS-INSU Tellus-Syster  
556 programme. We thank Sebastien Carretier and Odin Marc for fruitful discussions and Jens Turowski  
557 for his comments on a preliminary version of this manuscript. We thank Laure Guerit and an  
558 anonymous reviewer for their constructive comments which greatly improved the manuscript.

559

560

561 **References**

562 Amos, C.B., and Burbank, D.W.: Channel width response to differential uplift: *J. Geophys. Res.*, 112,  
563 doi:10.1029/2006JF000672, 2007.

564 Baynes, E.R.C., Lague, D., Attal, M., Gangloff, A., Kirstein, L.A., and Dugmore, A.J.: River self-  
565 organisation inhibits discharge control on waterfall migration: *Scientific Reports*, v. 8, p. 2444,  
566 doi:10.1038/s41598-018-20767-6, 2018.

567 Baynes, E.R.C., Lague, D., Steer, P., Bonnet, S., and Illien, L.: Sediment flux-driven channel  
568 geometry adjustment of bedrock and mixed gravel–bedrock rivers: *Earth Surface Processes and*  
569 *Landforms*, v. 45, p. 3714–3731, doi:10.1002/esp.4996, 2020.

570 Berlin, M.M., and Anderson, R.S.: Modeling of knickpoint retreat on the Roan Plateau, western  
571 Colorado: *Journal of Geophysical Research*, v. 112, p. F03S06, doi:10.1029/2006JF000553, 2007.

572 Bigi, A., Hasbargen, L.E., Montarani, A., and Paola, C.: Knickpoints and hillslope failure: Interactions  
573 in a steady-state experimental landscape, *in* Willet, C.D., Hovius, N., Brandon, M.T., and Fisher,  
574 D.M., eds. *Tectonics, Climate and Landscape evolution: Geological Society of America Special paper*  
575 398, p. 295-307, doi:10.1130/2006.2398(18), 2006.

576 Bonnet, S.: Shrinking and splitting of drainage basins in orogenic landscapes from the migration of the  
577 main drainage divide: *Nature Geoscience*, v. 2, p. 766–771, doi:10.1038/ngeo666, 2009.

578 Bonnet, S., and Crave, A.: Landscape response to climate change: Insights from experimental  
579 modeling and implications for tectonic versus climatic uplift of topography: *Geology*, v. 31, p. 123–  
580 126, doi: 10.1130/0091–7613, 2003.

581 Bufe, A., Paola, C., and Burbank, D.W.: Fluvial beveling of topography controlled by lateral channel  
582 mobility and uplift rate: *Nature geosc.*, 9, 706-710, doi:10.1038/ngeo2773, 2016.

583 Cantelli, A., and Muto, T.: Multiple knickpoints in an alluvial river generated by a single drop in base  
584 level: experimental investigation: *Earth Surface Dynamics*, 2, 271-278, doi:10.5194/esurf-2-271-2014,  
585 2014.



586 Carretier, S., Godderis, Y., Maertinez, J., Reich, M., and Martinod, J.: Colluvial deposits as a possible  
587 weathering reservoir in uplifting mountains: *Earth Surf. Dynam.*, 6, 217-237, doi: 10.5194/esurf-6-  
588 217-2018, 2018.

589 Cook, K.L., Turowski, J.M., and Hovius, N.: A demonstration of the importance of bedload transport  
590 for fluvial bedrock erosion and knickpoint propagation: *Earth Surface Processes and Landforms*, v. 38,  
591 p. 683–695, doi:10.1002/esp.3313, 2013.

592 Cook, K.L., Turowski, J.M., and Hovius, N.: River gorge eradication by downstream sweep erosion:  
593 *Nature geoscience*, doi:10.1038/NGEO2224, 2014.

594 Croissant, T., Lague, D., and Davy, P.: Channel widening downstream of valley gorges influenced by  
595 flood frequency and floodplain roughness: *Journal of Geophysical Research-Earth Surface*, v. 124, p.  
596 154–174, doi:10.1029/2018JF004767, 2019.

597 Crosby, B.T., and Whipple, K.X.: Knickpoint initiation and distribution within fluvial networks: 236  
598 waterfalls in the Waipaoa River, North Island, New Zealand: *Geomorphology*, v. 82, p. 16–38,  
599 doi:10.1016/j.geomorph.2005.08.023, 2006.

600 Davy, P., Croissant, T., and Lague, D.: A precipiton method to calculate river hydrodynamics, with  
601 applications to flood prediction, landscape evolution models, and braiding instabilities: *Journal of*  
602 *Geophysical Research-Earth Surface*, v. 122, p. 1491–1512, doi:10.1002/2016JF004156, 2017.

603 Duvall, A., Kirby, E., and Burbank, D.: Tectonic and lithologic controls on bedrock channel profiles  
604 and processes in coastal California: *Journal of Geophysical Research*, v. 109, p. F03002,  
605 doi:10.1029/2003JF000086, 2004.

606 Finnegan, N.J., Roe, G., Montgomery, D.R., and Hallet, B.: Controls on the channel width of rivers:  
607 Implications for modeling fluvial incision of bedrock: *Geology*, 33, 229-232, doi:10.1130/G21171.1,  
608 2005.

609 Finnegan, Noah J., Leonard S. Sklar, and Theodore K. Fuller. Interplay of sediment supply, river  
610 incision, and channel morphology revealed by the transient evolution of an experimental bedrock  
611 channel. *Journal of Geophysical Research: Earth Surface* 112.F3, doi:10.1029/2006JF000569, 2007.

612 Finnegan, N.J.: Interpretation and downstream correlation of bedrock river terrace treads created by  
613 propagation knickpoints: *Journal of Geophysical Research-Earth Surface*, v. 118,  
614 doi:10.1029/2012JF002534, 2013.

615 Fuller, T.K., Perg, L.A., Willenbring, J.K., and Lepper, K.: Field evidence of climate-driven changes  
616 in sediment supply leading to strath terrace formation: *Geology*, 37, 467-470,  
617 doi:10.1130/G25487A.1, 2009.

618 Fuller, T.K., Gran, K.B., Sklar, L.S., and Paola, C.: Lateral erosion in an experimental bedrock  
619 channel: The influence of bed roughness on erosion by bed load impacts: *Journal of Geophysical*  
620 *Research-Earth Surface*, v. 121, p. 1084-1105, doi:10.1002/2015JF003728, 2016.

621 Grimaud, J.-L., Paola, C., and Voller, V.: Experimental migration of knickpoints: influence of style of  
622 base-level fall and bed lithology: *Earth Surface Dynamics*, v. 4, p. 11–23, doi:10.5194/esurf-4-11-  
623 2016, 2016.

624 Hancock, G.S., and Anderson, R.S.: Numerical modeling of fluvial strath-terrace formation in  
625 response to oscillating climate: *Geological Society of America Bulletin*, v. 114, p. 1131-1142, 2002.

626 Hartshorn, K., Hovius, N., Dade, W.B., and Slingerland, R.L.: Climate-driven bedrock incision in an  
627 active mountain belt: *Science*, 297, 2036-2038, 2002.

628 Hasbargen, L.E., and Paola, C.: Landscape instability in an experimental drainage basin: *Geology*, v.  
629 24, p. 1067-1070, 2000.

630 Hasbargen, L.E., and Paola, C.: How predictable is local erosion rate in erosional landscape ? *in*  
631 Wilcox, P.R. and Iverson, R.M., eds., *Prediction in Geomorphology*: American Geophysical Union  
632 *Geophysical Monograph* 135, doi:10.1029/135GM16, 2003.

633 Kirby, E., and Whipple, K.X.: Expression of active tectonics in erosional landscapes: *Journal of*  
634 *Structural Geology*, v. 44, p. 54–75, doi:10.1016/j.jsg.2012.07.009, 2012.

635 Lague, D., Crave, A., and Davy, P.: Laboratory experiments simulating the geomorphic response to  
636 tectonic uplift: *Journal of Geophysical Research-Solid Earth*, v. 108, doi:10.1029/2002JB001785,  
637 2003.

638 Lague, D.: Reduction of long-term bedrock incision efficiency by short-term alluvial cover  
639 intermittency: *J. Geophys. Res.*, 115, doi:10.1029/2008JF001210, 2010.

640 Langston, A.L., and Tucker, G.E.: Developing and exploring a theory for the lateral erosion of  
641 bedrock channels for use in landscape evolution models: *Earth Surf. Dynam.*, 6, 1-27,  
642 doi:10.5194/esurf-6-1-2018, 2018.

643 Lavé, J., and Avouac, J.P.: Fluvial incision and tectonic uplift across the Himalayas of central Nepal:  
644 *Journal of Geophysical Research-Solid Earth*, v. 106, p. 26561–26591, doi:10.1029/2001JB000359,  
645 2001.

646 Li, T., Venditti, J.G., and Sklar, L.S.: An analytical model for lateral erosion from saltating bedload  
647 particle impacts: *J. Geophys. Res.— Earth*, 126, doi:10.1029/2020JF006061, 2021.

648 Mitchell, N.A., and Yanites, B.J.: Spatially variable increase in rock uplift in the Northern U.S.  
649 Cordillera recorded in the distribution of river knickpoint and incision depths: *Journal of Geophysical*  
650 *Research: Earth Surface*, v. 124, 1238-1260, doi:10.1029/2018JF004880, 2019.

651 Moussirou, B., and Bonnet, S.: Modulation of the erosion rate of an uplifting landscape by long-term  
652 climate change: An experimental investigation: *Geomorphology*, v. 303, p. 456–466,  
653 doi:10.1016/j.geomorph.2017.12.010, 2018.

654 Paola, C., Straub, K., Mohrig, D., and Reinhardt, L.: The “unreasonable effectiveness” of stratigraphic  
655 and geomorphic experiments: *Earth-Science Reviews*, v. 97, p. 1–43,  
656 doi:10.1016/j.earscirev.2009.05.003, 2009.

657 Rohais, S., Bonnet, S., and Eschard, R.: Sedimentary record of tectonic and climatic erosional  
658 perturbations in an experimental coupled catchment-fan system: *Basin Research*, v. 24, p. 198–212,  
659 doi:10.1111/j.1365-2117.2011.00520.x, 2012.

660 Scheingross, J.S., Lamb, M.P., and Fuller, B.M.: Self-formed bedrock waterfalls: *Nature*, v. 567, p.  
661 229–233, doi:10.1038/s41586-019-0991-z, 2019.

662 Schwanghart, W.S., and Scherler, D.: Divide mobility controls knickpoint migration on the Roan  
663 Plateau (Colorado, USA): *Geology*, 48, 698-702, doi:10.1130/G47054.1, 2020.

664 Singh, A., Reinhardt, L., and Fofoula-Georgiou, E.: Landscape reorganization under changing  
665 climatic forcing: Results from an experimental landscape: *Water Resources Research*, v. 51, p. 4320–  
666 4337, doi:10.1002/2015WR017161, 2015.

667 Sklar, L.S., and Dietrich, W.E.: Sediment and rock strength controls on river incision into bedrock:  
668 *Geology*, 29, 1087-1090, 2001.

669 Sweeney, K.E., Roering, J.J., and Ellis, C.: Experimental evidence for hillslope control of landscape  
670 scale: *Science*, v. 349, p. 51–53, doi:10.1126/science.aab0017, 2015.

671 Tofelde, S., Savi, S., Wickert, A. D., Bufer, A., and Schildgen, T. F.: Alluvial channel response to  
672 environmental perturbations: fill-terrace formation and sediment-signal disruption. *Earth Surface*  
673 *Dynamics*, v. 7, p. 609-631, doi:10.5194/esurf-7-609-2019, 2019.

674 Turowski, J.M., Lague, D., Crave, A., and Hovius, N.: Experimental channel response to tectonic  
675 uplift: *Journal of Geophysical Research-Earth Surface*, v. 111, doi:10.1029/2005JF000306, 2006.

676 Turowski, J.M., Lague, D., and Hovius, N.: Cover effect in bedrock abrasion: A new derivation and its  
677 implication for the modeling of bedrock channel morphology: *J. Geophys. Res.*, 112,  
678 doi:10.1029/2006JF000697, 2007.

679 Turowski, J.M., Hovius, N., Meng-Long, H., Lague, D., and Men-Chiang, C.: Distribution of erosion  
680 across bedrock channels: *Earth Surf. Process. Landforms*, 33, 353-363, doi:10.1002/esp.1559, 2008.

681 Turowski, J.M.: Alluvial cover controlling the width, slope and sinuosity of bedrock channels: Earth  
682 Surface Dynamics, v. 6, p. 29–48, doi:10.5194/esurf-6-29-2018, 2018.

683 Whipple, K.X., and Tucker, G.E.: Dynamics of the stream-power river incision model: Im- plications  
684 for height limits of mountain ranges, landscape response timescales, and research needs: Journal of  
685 Geophysical Research, v. 104, p. 17,661–17,674, 1999.

686 Whittaker, A.C., Cowie, P.A., Attal, M., Tucker, G.E., and Roberts, G.P.: Bedrock channel adjustment  
687 to tectonic forcing: Implications for predicting river incision rates: Geology, v. 35, p. 103,  
688 doi:10.1130/G23106A.1, 2007.

689 Whittaker, A.C., and Boulton, S.J.: Tectonic and climatic controls on knickpoint retreat rates and  
690 landscape response times: Journal of Geophysical Research, v. 117, F02024, doi:10  
691 .1029/2011JF002157, 2012.

692 Wickert, A.D., Martin, J.M., Tal, M., Kim, W., Sheets, B., and Paola, C.: River channel lateral  
693 mobility: Metrics, time scales, and controls: J. Geophys. Res.-Earth, 118, 396-412,  
694 doi:10.1029/2012JF002386, 2013.

695 Zavala-Ortiz, V., Carretier, S., Regard, V., Bonnet, S., Riquelme, R., and Choy, S.: Along-stream  
696 variations in valley flank erosion rates measured using  $^{10}\text{Be}$  concentrations in colluvial deposits from  
697 canyons in the Atacama Desert: Geophysical Research Letters, 48, doi:10.1029/2020GL089961, 2021.